



OPEN Subwavelength grating-assisted silicon nitride edge coupler with relaxed alignment tolerance

Yoon-Ho Sunwoo^{1,4}, Woo-Bin Lee^{1,4}, Yun-Jae Kwon¹, Chul-Soon Im², Ji-Yeong Gwon², Min-Cheol Oh³ & Sang-Shin Lee¹✉

We propose and realize a silicon nitride (SiN) edge coupler with enhanced alignment tolerance, achieved through the integration of a subwavelength grating (SWG) structure. The incident optical mode is guided from the SWG tri-tip to the main waveguide via two adiabatic transitions through intermediate bridge waveguides. The SWG tri-tip, composed of three laterally arranged SWG waveguides, provides a broader horizontal optical input region than a single-tip design, enhancing horizontal alignment tolerance. Moreover, careful engineering of the SWG period and fill factor lowers the effective index of the input waveguide compared to a solid waveguide, improving mode matching with optical fibers. The fabricated device demonstrates 1-dB alignment tolerances of $\pm 3 \mu\text{m}$ in the horizontal direction when coupled with a standard SMF-28 optical fiber, achieving a measured coupling efficiency of -3.8 dB/facet at 1550 nm wavelength. This horizontal tolerance is notably wider than that of conventional single-tip inverse-tapered edge couplers, validating the effectiveness of the SWG tri-tip design in expanding the input acceptance region. These results highlight the effectiveness of the proposed design in relaxing alignment sensitivity while maintaining efficient coupling, making it suitable for practical packaging and integration in SiN photonic platforms.

Keywords Subwavelength grating, Edge coupler, Alignment tolerance, Silicon nitride

The advent of AI data centers and high-performance computing necessitates innovations in data processing speed and transmission capacity. As conventional data links struggle to meet rising demands, optical interconnects have become essential to alleviate data transmission bottlenecks and reduce overall power consumption^{1–5}. Photonic integrated circuits (PICs) are crucial for implementing optical interconnects owing to their high integration density, complementary metal–oxide–semiconductor (CMOS) compatibility, broad bandwidth, and cost efficiency. This makes PICs a vital component in next-generation data centers and high-performance computing systems^{6–8}. Efficient fiber-to-chip coupling between external optical fibers and on-chip waveguides is critical for optimizing PIC performance^{9–12}. While silicon is widely used in PICs owing to its CMOS compatibility and high index contrast, its practical use is limited by strong nonlinear effects and a narrow transparency range. Alternatively, silicon nitride (SiN) has emerged as an attractive platform for PICs, owing to its low propagation loss, broad transparency window from the visible to the mid-infrared spectrum, and high-power handling capabilities^{13–15}. However, the relatively low index contrast leads to larger device footprints, complicating compact integration¹⁶. This low index contrast affects device size and fiber-to-chip coupling efficiency, which is highly dependent on the material platform. Optical coupling is primarily achieved through grating and edge couplers^{17,18}. Compared to grating couplers, which suffer from limited bandwidth and polarization dependence due to their diffractive nature¹⁹, edge couplers offer superior coupling efficiency, broader bandwidth, and reduced polarization sensitivity²⁰. However, edge couplers often have larger device footprints and tight alignment tolerance with optical fibers, which pose significant challenges for high-density photonic integration.

The implementation of edge couplers is primarily based on inverse-tapered waveguides, which enables adiabatic mode transition between the on-chip waveguide and input fiber. To achieve sufficient coupling efficiency, this structure typically requires taper lengths of several hundred micrometers, which increases device size^{21,22}. Multi-stage taper structures have been proposed to address footprint issues, where the taper is segmented into multiple stages with optimized geometries, effectively reducing the overall length²³. Nevertheless, these designs

¹Department of Electronic Engineering, Kwangwoon University, Seoul 01897, South Korea. ²Advanced Radar Team, Hanwha Systems Co., Ltd., Yongin 17121, South Korea. ³Department of Electronic Engineering, Pusan National University, Pusan (Busan) 46241, South Korea. ⁴Yoon-Ho Sunwoo and Woo-Bin Lee have equally contributed to this work. ✉email: slee@kw.ac.kr

still suffer from limited alignment tolerance. In contrast, multi-layer edge couplers enhance alignment tolerance by utilizing vertically stacked waveguides that gradually transform the mode profile along the propagation axis^{24–26}. However, their structural complexity and fabrication challenges can hinder scalability and integration with standard platforms. Recent research has focused on subwavelength grating (SWG) structures to resolve these challenges^{27–34}. SWG structures consist of alternating high- and low-index segments with a period smaller than the operating wavelength, enabling the waveguide to function as an effective medium with a tunable refractive index^{35,36}. By fine-tuning the grating period and fill factor, the effective index of the waveguide can be engineered to closely match the mode field characteristics of standard single-mode fibers. This enhanced mode matching allows for compact designs and relaxed alignment tolerances. However, most SWG-based edge couplers have been mostly implemented on a silicon photonic platform rather than on its SiN counterpart, which offers distinct advantages such as a wider transparency window and lower propagation loss. Moreover, the inherently low nonlinearity and low index contrast of SiN enable relaxed fabrication tolerance and reduced phase errors, further highlighting its application toward robust fiber-to-chip coupling^{13–15}. Although the relatively low index contrast of the SiN platform can facilitate mode-field expansion through inverse taper structures, the exploitation of an SWG structure helps enhance the performance within a shorter device length³⁷ and extend the design concept to other photonic platforms, thereby exhibiting intermediate refractive indices.

In this study, we propose an SiN-based edge coupler incorporating a SWG tri-tip structure at the input facet where it interfaces with an optical fiber. The SWG waveguide is designed with a carefully engineered grating period and fill factor, enabling a reduced effective index compared to conventional solid waveguides. This index tailoring facilitates improved mode matching with standard single-mode fiber. The SWG tips are arranged in a trident configuration, providing a wider lateral coupling interface than a single-tip design thereby enhancing alignment tolerance with the input fiber. The optical mode from an SMF-28 fiber, which has a large mode field diameter (MFD), is coupled into the SWG tri-tip, followed by an adiabatic transition into the main waveguide. This configuration minimizes mode distortion and insertion loss while significantly reducing the overall footprint. The proposed edge coupler is fully compatible with standard CMOS fabrication processes and enhances alignment tolerance, making it a promising candidate for robust fiber-to-chip coupling in large-scale PICs.

Proposed SWG-assisted SiN edge coupler

Figure 1 illustrates the schematic of the proposed SiN edge coupler integrated with the SWG structure. The proposed edge coupler comprises three functional sections: SWG tri-tip, adiabatic coupler 1, and adiabatic coupler 2. Input light from the SMF-28 fiber is symmetrically coupled into three parallel SWG tips. This trident configuration effectively broadens the horizontal optical input region compared to a single-tip design, thereby improving horizontal alignment tolerance. Each SWG comprises a periodic structure with subwavelength pitch, forming a homogeneous waveguide with a uniform effective refractive index (n_{eff}) based on the effective medium theory^{35,36}. In contrast to conventional solid waveguide tips, the SWG tips could exhibit a lower effective refractive index, reducing mode mismatch at the fiber-waveguide interface and facilitating smoother optical mode transitions. The three SWG waveguides are arranged in a straight collinear configuration along the propagation axis, ensuring identical optical path lengths. This phase-matched layout minimizes phase mismatch among guided beams, enhancing constructive interference and improving broadband robustness. The guided mode excited from the SWG tri-tip is then adiabatically transferred to the adjacent bridge waveguides via adiabatic coupler 1, reducing reflection and mode distortion. Finally, the two bridge waveguides merge into the main waveguide via a symmetric taper, designed as adiabatic coupler 2, enabling gradual optical power combining with minimal loss and efficient confinement within the main waveguide.

As shown in Fig. 2a, the SiN waveguide is constructed on a silicon substrate with a buried oxide layer. The SiN core thickness (t_{SiN}) is 400 nm, while the buried oxide layer and top oxide cladding have thicknesses of 4.5 and 3 μm , respectively, providing complete encapsulation of the waveguide. Figure 2b details the layout of the proposed edge coupler, which is defined by a set of geometric parameters. L_{total} denotes the total device

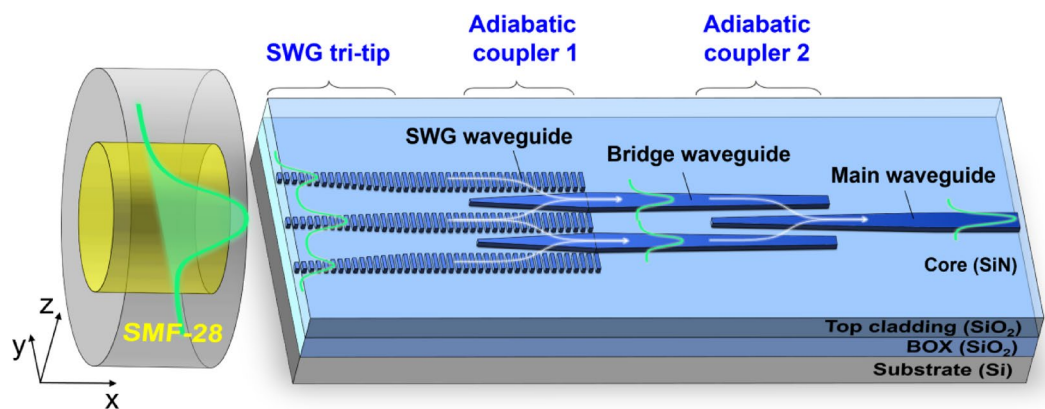


Fig. 1. Configuration of the proposed subwavelength grating (SWG)-assisted silicon nitride (SiN) edge coupler.

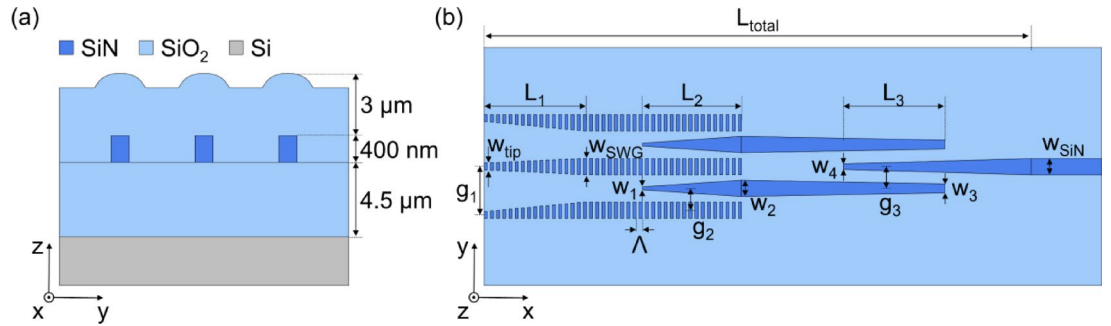


Fig. 2. (a) Cross-section of the SWG tri-tip. (b) Schematic of the proposed edge coupler.

L_{total}	L_1	L_2	L_3	Λ	w_{tip}	w_{SWG}	w_{SiN}
110 μm	60 μm	20 μm	14 μm	400 nm	200 nm	1 μm	1 μm
w_1	w_2	w_3	w_4	g_1	g_2	g_3	
200 nm	700 nm	600 nm	600 nm	3 μm	1.2 μm	1.1 μm	

Table 1. Structural parameters of the designed edge coupler.

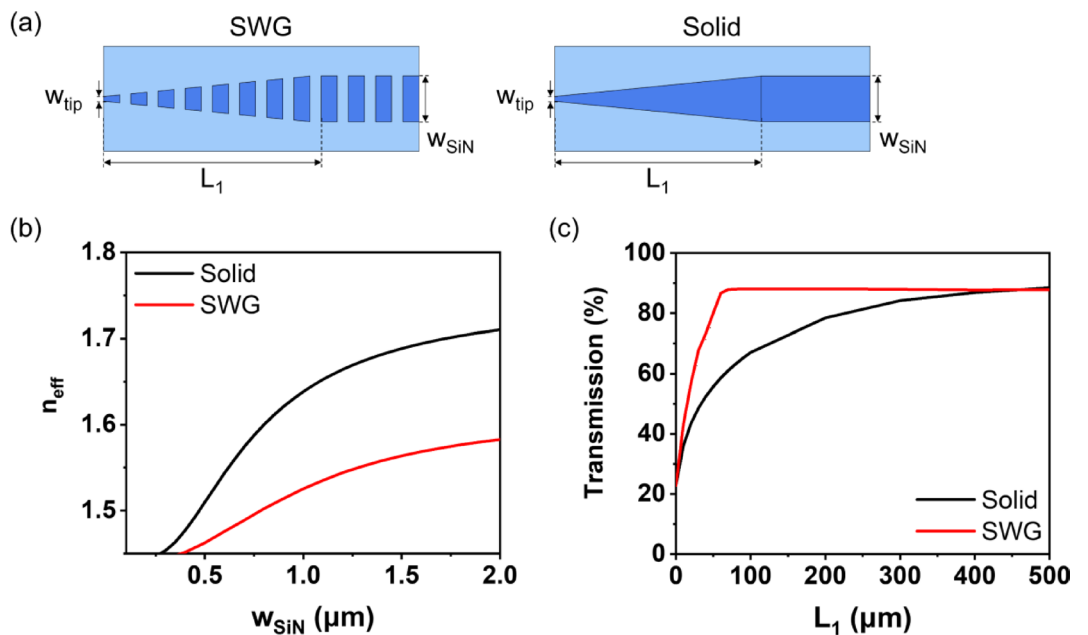


Fig. 3. Schematic of (a) the SWG (left) and solid (right) taper waveguide. (b) Effective refractive index (n_{eff}) of the SWG and solid waveguide according to the waveguide width at a wavelength of 1550 nm. (c) Transmission according to the taper length of SWG and solid waveguide at a wavelength of 1550 nm.

length, while L_1 , L_2 , and L_3 represent the lengths of the SWG tri-tip, adiabatic coupler 1, and adiabatic coupler 2, respectively. The SWG grating period is given by Λ , and the taper tip width of the SWG tip is labeled by w_{tip} . w_{SWG} and w_{SiN} refer to the widths of the SWG and main waveguides, respectively. For the bridge waveguide, w_1 , w_2 , and w_3 represent the taper widths at different transition regions, while w_4 denotes the taper tip width of the main waveguide. g_1 , g_2 , and g_3 , correspond to the inter-SWG tip spacing, the gap between the SWG and bridge waveguide, and the gap between the bridge and main waveguides, respectively. All corresponding values are summarized in Table 1.

SWG tri-tip

To implement the SWG tri-tip, a trident-shaped taper tip based on SWG waveguides was employed. Figure 3a compares the inverse-tapered waveguide structures realized with SWG and solid waveguides. The SWG consists of a periodic grating structure with a 400 nm pitch and a fill factor of 0.625, which is smaller than the operating

wavelength. According to effective medium theory, when the grating period is sufficiently subwavelength, the structure does not support higher-order harmonics and can be regarded as a homogeneous medium with a uniform n_{eff} . This enables the SWG waveguide to function as an effective core with tailored optical properties, facilitating mode matching with the optical fiber. As depicted in Fig. 3b, the n_{eff} of the fundamental transverse electric (TE) mode increases with the SiN waveguide width w_{SiN} ; however, the SWG taper exhibits a slower rate of change than the solid taper. The n_{eff} values were calculated using the finite-difference eigenmode solver (ANSYS Lumerical). Generally, inverse-tapered waveguides require a sufficiently long taper length to gradually transform the n_{eff} , thereby suppressing higher-order mode excitation and minimizing transition loss. Owing to the reduced index sensitivity to waveguide width, the SWG taper enables efficient mode transition with a significantly shorter taper length. This is because, for the same waveguide width, the SWG exhibits a lower effective refractive index than its solid counterpart, reducing mode mismatching effects over shorter distances. The transmission characteristics were computed using the 3D beam propagation method (Synopsys RSoft). As shown in Fig. 3c, the simulation results indicate that a 60- μm -long SWG taper achieves a transmission of 87%, which is comparable to that of a 500- μm -long solid taper. These results demonstrate the effectiveness of the proposed compact SWG taper design in minimizing footprint while maintaining high transmission. As demonstrated in Figs. 4a and b, the SWG tri-tip exhibits a broader lateral mode field profile compared to the single-tip structure, leading to improved spatial matching with the fiber mode. The modal area of the SMF-28 fiber is 85.5 μm^2 , which is closer to that of the SWG tri-tip of 71.1 μm^2 than that of the single-tip, which is 55.2 μm^2 , further supporting the enhanced mode matching of the proposed structure. As shown in Fig. 4c, the modal overlap varies with the w_{tip} in the range of 50–200 nm. For $w_{\text{tip}} = 200$ nm, the proposed SWG tri-tip and the single-tip design achieved similar modal overlap values of 89% and 88% with the SMF-28 fiber mode, respectively. Overall, it was observed that the SWG-assisted structure provides higher overlap across the entire range than the single-tip design, demonstrating significant robustness against variations in tip width.

Adiabatic couplers

Adiabatic coupler 1 is designed for inducing efficient mode transition from the SWG to the bridge waveguides with minimal loss. As illustrated in Fig. 5a, a tri-SWG-to-solid transition structure models the mode evolution. The gap between the SWG and bridge waveguides was set to 1.2 μm , and the output width of the bridge waveguide was 700 nm. Using 3D finite-difference time-domain (FDTD) simulations (ANSYS Lumerical), the transition efficiency was calculated as a function of L_2 for various w_1 values, as shown in Fig. 5b. The transition efficiency was evaluated when the input mode with a tri-peak intensity distribution along the SWG waveguides is coupled into the bridge waveguides with a double-peak profile. A larger w_1 results in stronger fluctuations in transmission efficiency across coupling lengths, likely owing to weaker mode confinement and less adiabatic mode transition, which can induce partial back-coupling into the SWG waveguide. When $w_1 = 200$ nm, the transition efficiency reaches 89% at $L_2 = 20$ μm , confirming effective power transfer within a compact transition length.

Figure 6a depicts adiabatic coupler 2, which integrates guided modes emerging from the two bridge waveguides into the main waveguide. The gap between the bridge and main waveguides is fixed at 1.1 μm . Figure 6b shows the transition efficiency calculated as a function of w_4 and L_3 using the eigenmode expansion solver (ANSYS Lumerical). The simulation results indicate a maximum transition efficiency of 99% when $w_4 = 600$ nm and $L_3 = 14$ μm , confirming low-loss optical power combining via an optimally designed symmetric taper. Unlike adiabatic coupler 1, adiabatic coupler 2 exhibits greater sensitivity to coupling length, with fluctuations in transmission as L_3 increases, which is mostly due to incomplete unilateral coupling between the main waveguide

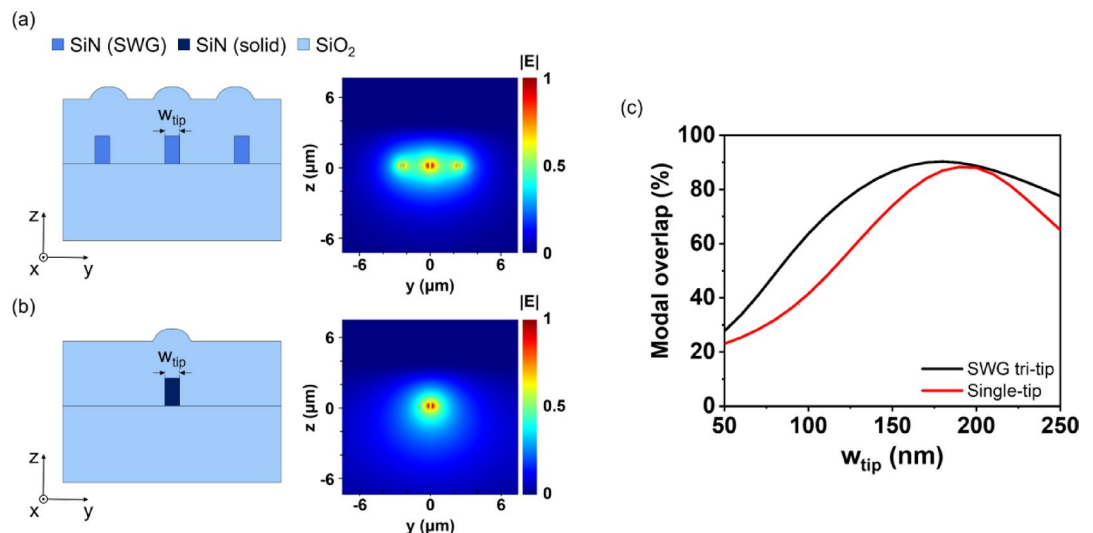


Fig. 4. Schematic and cross-section mode profile of (a) the SWG tri-tip and (b) single-tip structure. (c) Calculated modal overlap in terms of the taper tip width at a wavelength of 1550 nm.

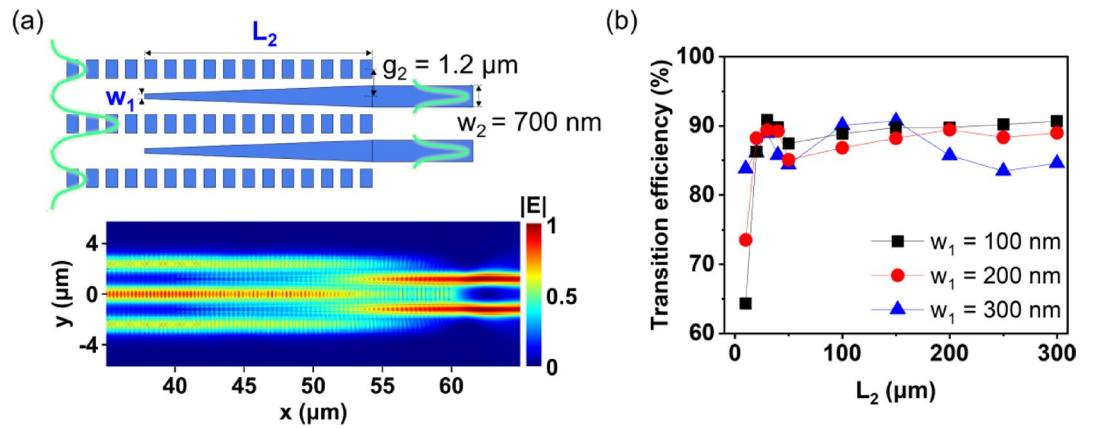


Fig. 5. (a) Schematic and electric field distribution of the adiabatic coupler 1 and (b) simulated adiabatic transition efficiency according to the coupling length at a wavelength of 1550 nm.

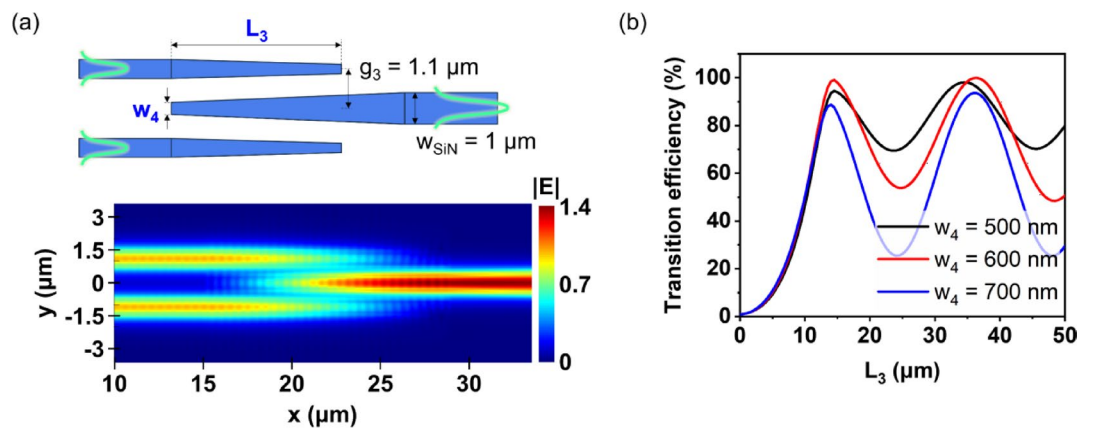


Fig. 6. (a) Schematic and electric field distribution of the adiabatic coupler 2. (b) Simulated adiabatic transition efficiency according to the coupling length at a wavelength of 1550 nm.

and bridge waveguides. The design can potentially be optimized by incorporating SWG waveguides, but with added structural complexity.

SWG-assisted SiN edge coupler

Figure 7a illustrates the simulated electric field distribution of the proposed SWG-assisted SiN edge coupler, based on the optimized parameters from the preceding designs. The input mode from the SMF-28 fiber, with an MFD of 10 μm in terms of $1/e^2$ intensity level, is mode-matched and symmetrically coupled into the SWG tri-tip, ensuring efficient optical power injection and minimal reflection at the fiber-to-chip interface. The guided mode profile of the SMF-28 fiber is depicted in Fig. 7b. Figure 7c presents cross-sectional electric field distributions $|E|$ at various x positions (0, 30, 60, 70, 90, and 110 μm), demonstrating even optical power distribution among the three SWG waveguides, adiabatically transitioning to the bridge waveguides, and merging into the main waveguide. The gradual mode evolution along the coupler confirms adiabatic transition with negligible scattering and distortion, validating the efficiency and robustness of the design. As shown in Fig. 8a, the coupling efficiency was calculated at a wavelength of 1550 nm through 3D FDTD simulations by varying the fill factor from 0.3 to 0.8 in steps of 0.1 and the grating period from 300 to 500 nm in steps of 25 nm, with other parameters fixed. To satisfy the subwavelength condition, the grating period was designed to be smaller than the guided half-wavelength³⁸. The results indicate that smaller fill factors and shorter grating periods generally led to higher coupling efficiency, owing to improved effective index matching and mode transition. The proposed edge coupler was designed with a fill factor of 0.625 and a grating period of 400 nm, considering a trade-off between efficiency and manufacturability as well as fabrication tolerance. Figure 8b presents the calculated coupling efficiencies between an SMF-28 fiber and the proposed SWG-assisted SiN edge coupler and a conventional single-tip edge coupler, designed with the same length of 110 μm . At a wavelength of 1550 nm, the proposed SWG tri-tip design achieved a coupling efficiency of -1.6 dB/facet, whereas the single-tip design exhibits -3.0 dB/facet. The results imply that the SWG-assisted coupler improves the coupling efficiency and maintains a stable spectral response over the entire wavelength range. While the proposed edge coupler was optimized for the TE mode,

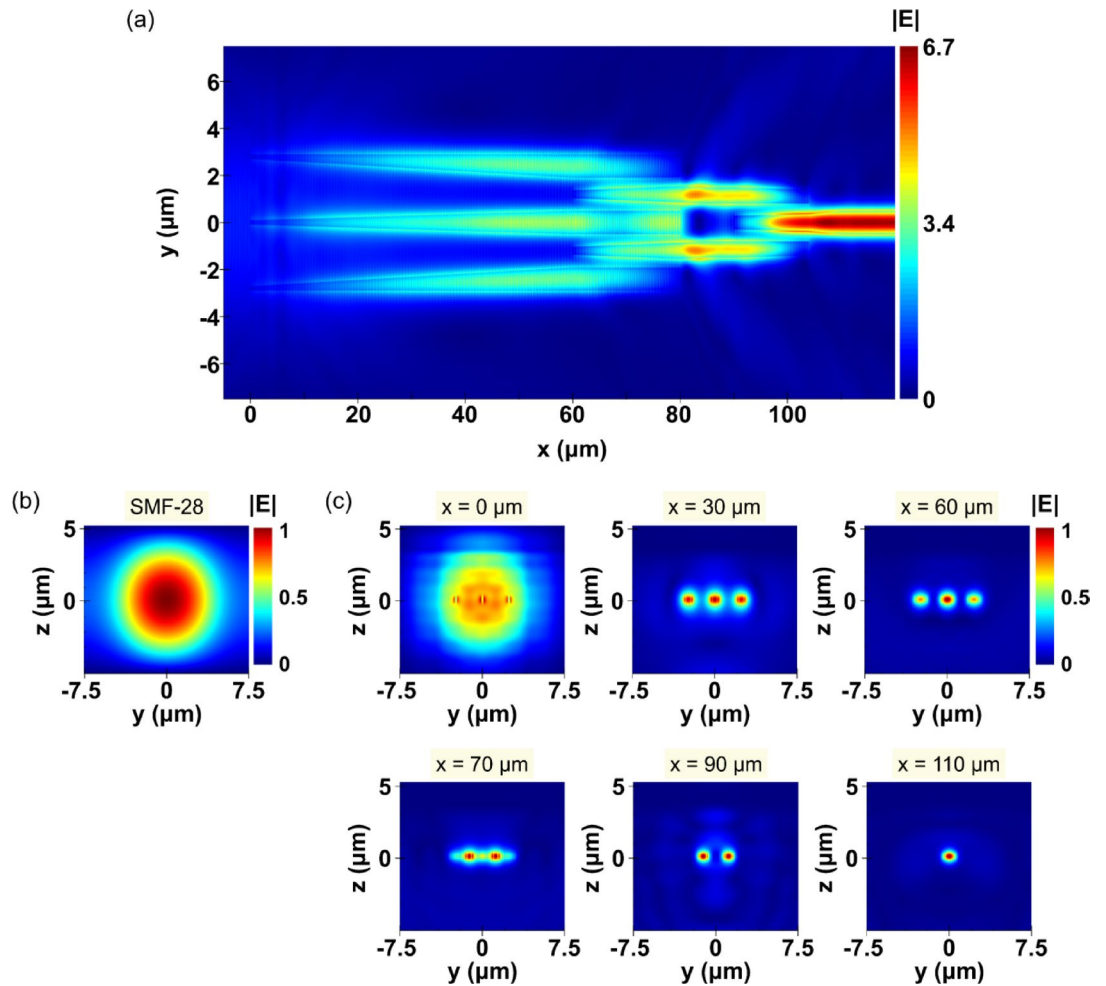


Fig. 7. (a) Electric field distribution of the proposed SWG-assisted SiN edge coupler at a wavelength of 1550 nm. (b) Guided mode profile of the SMF-28 fiber. (c) Cross-sectional electric field profiles at various x positions ($x=0, 30, 60, 70, 90, 110 \mu\text{m}$).

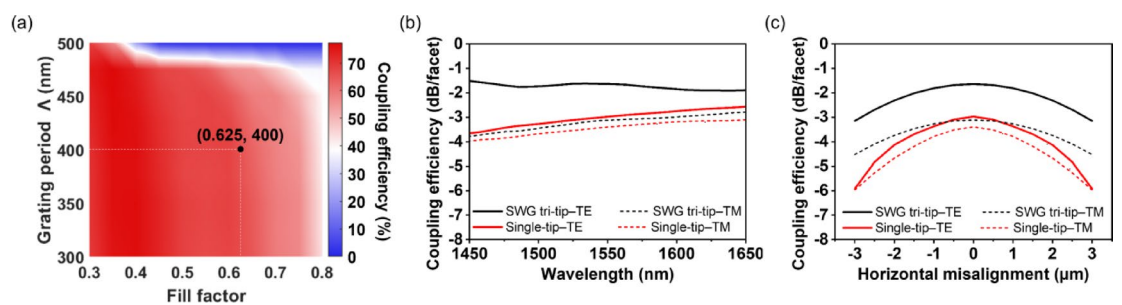


Fig. 8. (a) Simulated coupling efficiency between the SMF-28 fiber and SWG-assisted SiN edge coupler as a function of the fill factor and grating period of SWG at a wavelength of 1550 nm. (b) Simulated coupling efficiency of the proposed edge coupler and conventional single-tip edge coupler with an SMF-28 fiber over a wavelength range of 1450–1650 nm, and (c) coupling efficiency as a function of horizontal misalignment at a wavelength of 1550 nm.

the transverse magnetic (TM) mode coupling efficiency was also evaluated, to exhibit -3.1 dB/facet for the SWG tri-tip and -3.4 dB/facet for the single-tip structure. The back-reflection at the fiber-to-chip interface was also calculated through 3D FDTD simulations to exhibit a return loss of about 25.4 dB. Figure 8c shows the coupling efficiency as a function of horizontal misalignment between the fiber and edge coupler. The 1-dB alignment tolerance in the horizontal direction was $\pm 3 \mu\text{m}$ for the proposed structure and approximately $\pm 2 \mu\text{m}$ for the

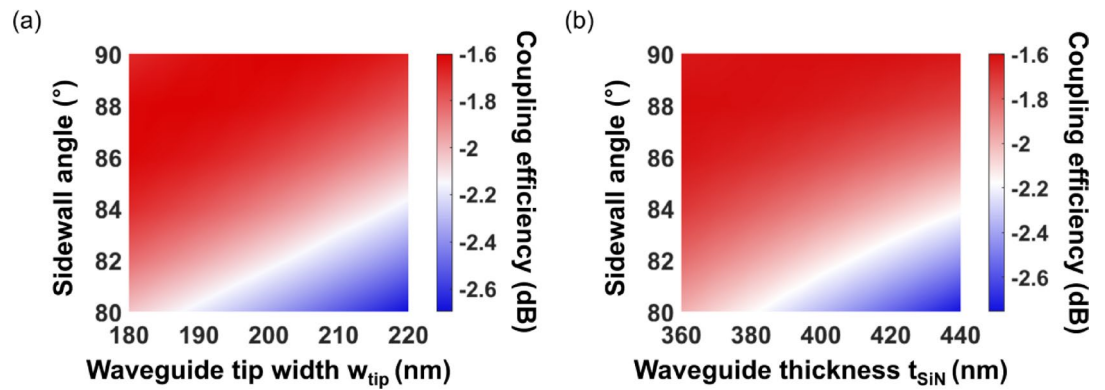


Fig. 9. Calculated coupling efficiency between the input fiber and SiN waveguide as a function of w_{tip} , t_{SiN} , and sidewall angle of the fabricated device at a wavelength of 1550 nm for the fundamental TE mode. (a) Coupling efficiency with $t_{\text{SiN}} = 400$ nm. (b) Coupling efficiency with $w_{\text{tip}} = 200$ nm.

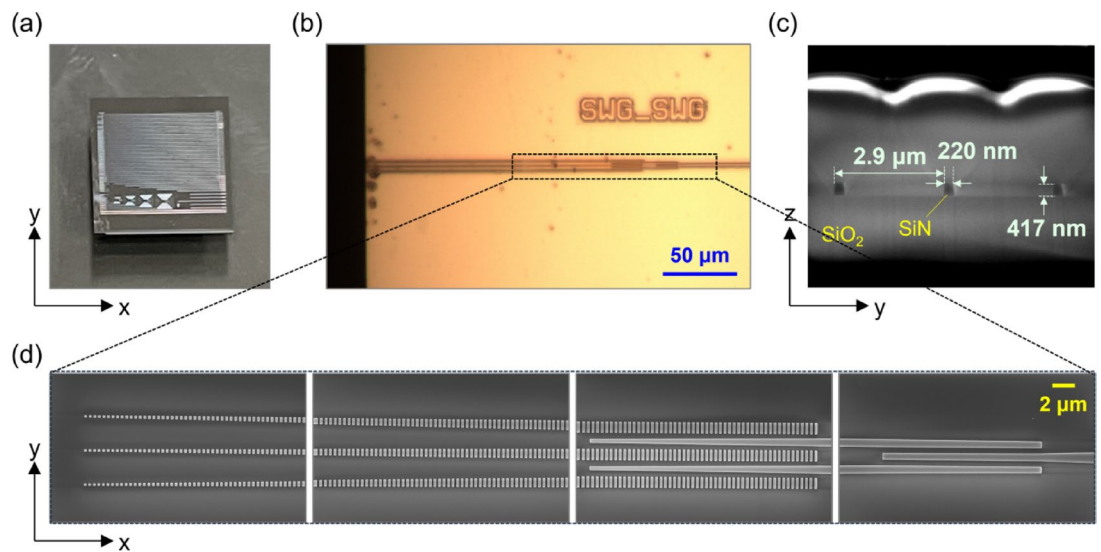


Fig. 10. (a) Optical image of the fabricated device. (b) Optical microscope images of the fabricated SWG-assisted SiN edge coupler. Scanning electron microscope image of (c) cross-section of the SWG tri-tip and (d) SWG-assisted SiN edge coupler.

single-tip structure, demonstrating a relaxed alignment sensitivity compared to the conventional edge couplers for both TE and TM modes. In consideration of fabrication errors, the coupling efficiency between the proposed edge coupler and optical fiber was calculated for variations in the SiN waveguide geometry, including w_{tip} , t_{SiN} , and sidewall angle, as shown in Figs. 9a and b. The simulations were performed for the fundamental TE mode at a wavelength of 1550 nm, and the results in Fig. 9a were calculated with t_{SiN} fixed at 400 nm, and those in Fig. 9b were calculated with w_{tip} fixed at 200 nm. With reference to the nominal design parameters ($w_{\text{tip}} = 200$ nm, $t_{\text{SiN}} = 400$ nm), the coupling efficiency variations were evaluated for $\pm 10\%$ dimensional deviations. The most unfavorable case occurs when both w_{tip} and t_{SiN} increase by 10% and the sidewall angle is 80°, resulting in an excess coupling loss of ~ 1 dB relative to the ideal case.

Fabrication and characterization of the SWG-assisted SiN edge coupler

Figure 10a shows the optical image of the fabricated photonic chip, built using a planar lightwave circuit platform provided by Applied Nanotools Inc. (ANT, Canada), with direct-write electron-beam lithography used for defining the SiN waveguide structures. The fabrication process offered by ANT ensures a minimum feature size and spacing of 120 nm, with a dimensional tolerance of ± 20 nm, which is sufficient to implement the SWG structures employed in this study reliably. Figure 10b presents a microscope image of the SWG-assisted SiN edge coupler, clearly illustrating its entire functional structure, including the SWG tri-tip, adiabatic coupler 1, and adiabatic coupler 2. Figure 10c provides a cross-sectional scanning electron microscope image of the SWG tri-tip. The gap between adjacent SWG tips is approximately 2.9 μm, while the SWG tip width, thickness, and sidewall angle measure 220, 417 nm, and 88°, respectively, closely matching design specifications. Considering the

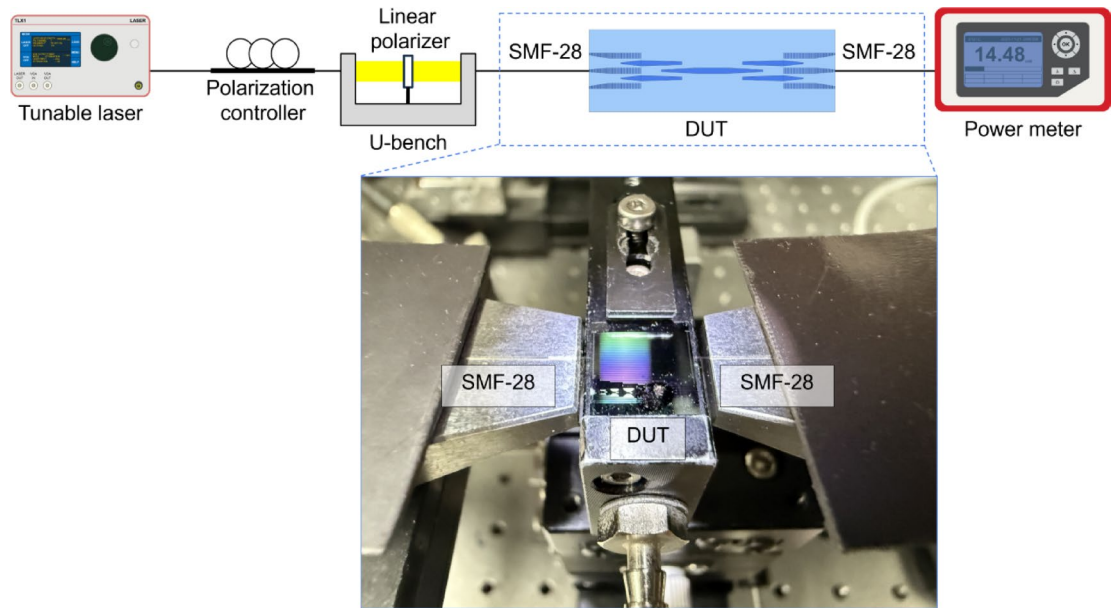


Fig. 11. Experimental setup for measuring the coupling efficiency between the SMF-28 fiber and SWG-assisted SiN edge coupler.

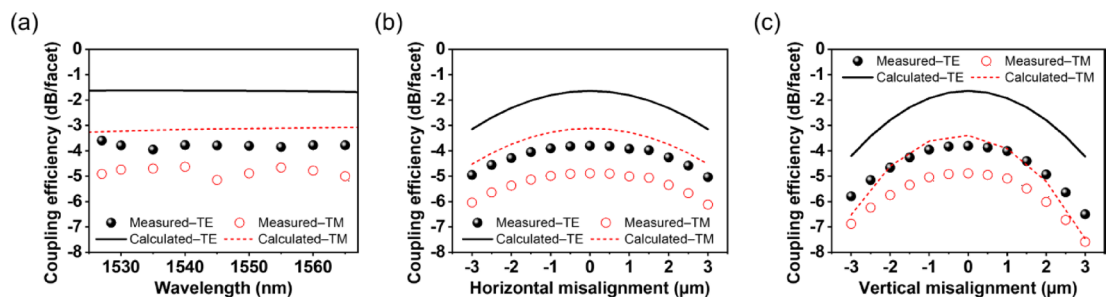


Fig. 12. (a) Calculated and measured coupling efficiency of the proposed edge coupler to an SMF-28 fiber. Alignment tolerances between the SMF-28 fiber and proposed edge coupler in (b) horizontal and (c) vertical directions at a wavelength of 1550 nm.

fabrication errors analyzed in Fig. 9, an additional coupling loss of ~ 0.1 dB is expected for the fabricated device. Figure 10d presents top-view scanning electron microscope image of the fabricated edge coupler, demonstrating excellent structural integrity and adherence to design dimensions. The input and output facets were polished for smooth, well-defined surfaces, crucial for efficient fiber-to-chip coupling. Figure 11 shows the experimental setup used to characterize the fiber-to-chip coupling efficiency of the SWG-assisted SiN edge coupler. A tunable laser source (TLX1, Thorlabs) was employed to launch continuous-wave light into an input SMF-28 fiber, with its polarization adjusted using a polarization controller (STPC-A-FA, KS Photonics) in combination with a linear polarizer (FBR-AH3, Thorlabs) to excite the fundamental TE guided mode. The input and output fibers were initially aligned to the facets of the device under test using a motorized stage equipped with a top-view camera. The fibers were then finely adjusted to maximize the transmitted optical power through an optical power meter (PM100D, Thorlabs), thereby determining the optimal coupling position.

Figure 12 presents the measured and simulated coupling efficiency of the SWG-assisted SiN edge coupler interfaced with a standard SMF-28 fiber. In Fig. 12a, the measured coupling efficiency is stable over the C-band wavelength range (1527–1565 nm), exhibiting -3.8 dB/facet on average for the TE mode at a wavelength of 1550 nm. Due to equipment limitations, the experimental characterization was primarily performed over the C-band, while the calculated results in Fig. 8b cover a broader wavelength range (1450–1650 nm), confirming the broadband characteristics of the proposed edge coupler. The discrepancy from the calculated value of -1.6 dB/facet was attributed to the excess loss incurred by the elongated tip length (L_{tip}) included in the fabricated device, as analyzed in Figs. 13a and b. The SWG tri-tip region of the fabricated device had an elongated length of $L_{\text{tip}} = 150$ μm , while the portion of the taper tip was practically left unpolished to avoid structural damage during the manual polishing process. The facet has been manually polished using a NOVA polishing system (KrellTech, USA) to expose the coupling interface. The coupling efficiency with the elongated L_{tip} was analyzed

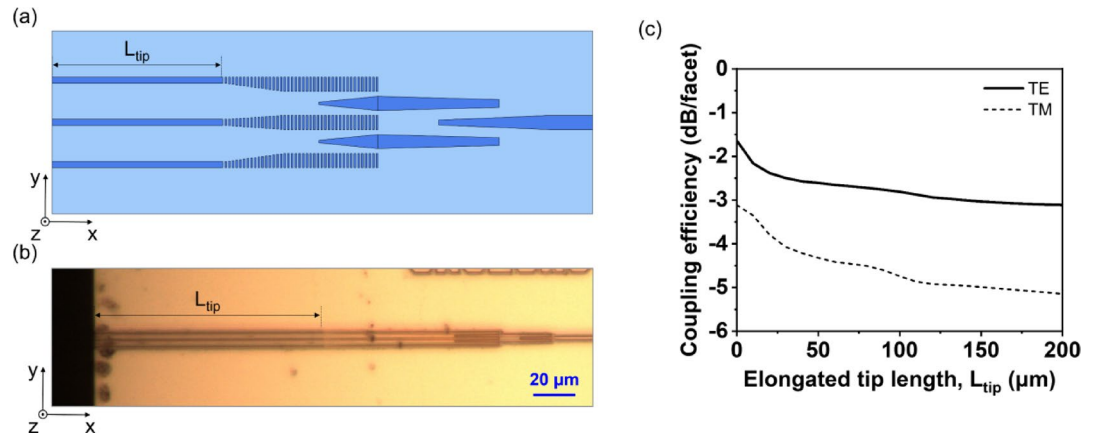


Fig. 13. (a) Schematic and (b) optical microscope image of the fabricated SWG-assisted edge coupler with an elongated tip. (c) Calculated coupling efficiency between the proposed SWG-assisted edge coupler and SMF-28 fiber based on the elongated tip length at a wavelength of 1550 nm.

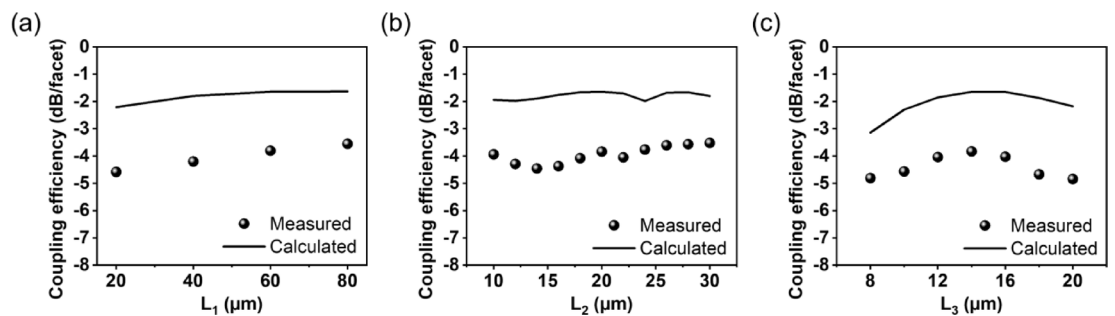


Fig. 14. Calculated (black line) and measured (black dot) coupling efficiency according to the length of (a) SWG tri-tip, (b) adiabatic coupler 1, and (c) adiabatic coupler 2 at a wavelength of 1550 nm.

through 3D FDTD simulations, as shown in Fig. 13c, where the loss increases with L_{tip} as part of the large MFD of the input fiber undesirably penetrates the Si substrate. To mitigate this issue, L_{tip} may be reduced at the design stage, or the elongated taper can be further shortened through a more precise polishing process. In future work, higher coupling efficiency can be achieved by taking advantage of a deep-trench process provided by ANT, which enables direct access to the SWG tip at the chip edge, or by incorporating microscopically visible ruler patterns into the coupler region to facilitate precisely controlled polishing in accordance with the desired position. Figures 12b and c show the horizontal and vertical alignment tolerance at 1550 nm, respectively. The 1-dB alignment tolerance measures approximately $\pm 3 \mu\text{m}$ horizontally and $\pm 2 \mu\text{m}$ vertically, validating the relaxed alignment tolerance achieved by the symmetric SWG tri-tip and taper configuration. These values represent a notable improvement over conventional inverse-tapered edge couplers, which typically exhibit narrower alignment margins, especially in the horizontal direction. The slight degradation in the measured coupling efficiency compared to the simulation is attributed mostly to fabrication-induced imperfections, such as sidewall roughness, non-vertical sidewall angles, and deviations in grating geometry, which can cause mode mismatch and additional scattering losses³⁹. Figure 14 examines the sensitivity of overall coupling efficiency to the key design parameters. The results were obtained by varying each structural parameter individually while maintaining the other parameters fixed at the design values listed in Table 1. In Fig. 14a, coupling efficiency increases with the length of the SWG tri-tip (L_1), plateauing near the standard value of 60 μm , which ensures sufficient mode transition with a minimal footprint. Figure 14b shows the importance of the length of adiabatic coupler 1 (L_2), with optimal performance achieved around 20 μm , minimizing back-reflection and ensuring efficient mode transition. In Fig. 14c, coupling efficiency is maximum when the length of adiabatic coupler 2 (L_3) is 14 μm , confirming the effectiveness of the symmetric and compact layout. Overall, the measured data exhibited good agreement with the simulation results, validating the robustness of the proposed design and its tolerance against fabrication variations.

The proposed edge coupler incorporates a SWG tri-tip structure at the input facet. The number of SWG tips can be increased beyond three to improve lateral alignment tolerance, and additional transitions from the outer tips to the central waveguide could engender undesired optical losses. Consequently, this trade-off between the alignment robustness and insertion loss should be cautiously managed during design. As shown in Fig. 14, coupling efficiency is found to be most sensitive to variations in L_3 , likely due to incomplete mode coupling

References	Configuration	MFD of optical fibers ($1/e^2$; μm)	Coupling efficiency (TE/TM; dB/facet)	1-dB alignment tolerance (horizontal/vertical; μm)	3-dB bandwidth (nm)	Coupler length (μm)	Material
20	Multi-layer	10.4	-0.75/NA	$\pm 2.2/\pm 2.2$	> 150	260	Si/SiN
21	Multi-layer	10.4	-0.6/-0.6	$\pm 2/\pm 2$	NA	2100	High-index doped silica glass/SiN
23	Multi-stage taper	4	-0.36/-0.56	$\pm 1/\pm 1$	> 965	76	SiN
24	Multi-layer array	10.4	-0.49/-0.92	NA	> 160	1200	Si/SiN
27	SWG	10.4	-2.22/-2.53	NA	120	90	Si
28	SWG	3.2	-0.9/-1.2	NA	> 100	NA	Si
29	Multi-layer/SWG	10.4	-0.86/-0.94	$\pm 2.5/\pm 1.8$	> 100	550	Si/SiN
30	SWG	3.2	-0.23	NA	> 390	60	Si
31	SWG	3.2	-1.0/NA	$\pm 1/\pm 0.5$	> 100	75	Si
This work	SWG	10.4	-3.8/-4.9 *	$\pm 3/\pm 2$	> 200	110	SiN

Table 2. Comparison of the various types of edge couplers. * The measured coupling efficiency includes an unwanted loss of ~ 2.0 dB due to the elongated tip, while the simulated results are -1.6 and -3.1 dB/facet for the TE and TM cases, respectively.

between the bridge and main waveguides, resulting in interference effects. Incorporating SWG structures within adiabatic coupler 2 may enhance tolerance to length deviations and improve coupling efficiency. The proposed coupler was compared with previously reported edge couplers in terms of the configuration, coupling efficiency, 1-dB alignment tolerance, 3-dB bandwidth, coupler length, and material, as summarized in Table 2.

Conclusion

In this study, we experimentally demonstrated an alignment-tolerant SiN edge coupler incorporating SWG structures. The proposed coupler comprises three integrated sections: a SWG tri-tip for horizontal mode expansion, and two adiabatic couplers that sequentially transfer the guided mode from the SWG tri-tip to the bridge waveguides, and subsequently to the main waveguide, all within a total length of as short as $110 \mu\text{m}$. The measured 1-dB alignment tolerance of $\pm 3 \mu\text{m}$ with SMF-28 fiber represents a substantial improvement over that of a conventional inverse-tapered edge coupler, confirming the robustness of the SWG tri-tip layout for relaxed fiber positioning. The coupling efficiency was measured to be -3.8 dB/facet at a wavelength of 1550 nm , closely aligning with results from 3D FDTD simulations when the elongated tip length of the fabricated device was considered. These results validate the effectiveness of the proposed SWG-assisted coupler architecture in achieving a compact footprint and enhanced alignment tolerance. The proposed design provides a promising pathway for robust and scalable fiber-to-chip coupling in SiN-based PICs, particularly for applications requiring high packaging tolerance and reduced fabrication complexity.

Data availability

The datasets generated and/or analyzed during the current study are available from the corresponding author upon reasonable request.

Received: 11 September 2025; Accepted: 28 October 2025

Published online: 19 November 2025

References

- Kachris, C. & Tomkos, I. A survey on optical interconnects for data centers. *IEEE Commun. Surv. Tutor.* **14**(4), 1021–1036 (2012).
- Taubenblatt, M. A. Optical interconnects for high-performance computing. *J. Lightwave Technol.* **30**(4), 448–458 (2012).
- Biberman, A. & Bergman, K. Optical interconnection networks for high-performance computing systems. *Rep. Prog. Phys.* **75**, 046402 (2012).
- Rumley, S. et al. Optical interconnects for extreme scale computing systems. *Parallel Comput.* **64**, 65–80 (2017).
- Young, I. A. et al. Optical technology for energy efficient I/O in high performance computing. *IEEE Commun. Mag.* **48**(10), 184–191 (2010).
- Helkey, R., Saleh, A. A. M., Buckwalter, J. & Bowers, J. E. High-performance photonic integrated circuits on silicon. *J. Lightwave Technol.* **25**(5), 8300215 (2019).
- Dong, P., Chen, Y.-K., Duan, G.-H. & Neilson, D. T. Silicon photonic devices and integrated circuits. *Nanophotonics* **3**(4–5), 215–228 (2014).
- Xiang, C. et al. High-performance silicon photonics using heterogeneous integration. *IEEE J. Sel. Top. Quantum Electron.* **28**(3), 8200515 (2022).
- Alder, T., Stöhr, A., Heinzlmann, R. & Jäger, D. High-efficiency fiber-to-chip coupling using low-loss tapered single-mode fiber. *IEEE Photonics Technol. Lett.* **12**(8), 1016–1018 (2000).
- Khan, S. et al. Low-loss, high-bandwidth fiber-to-chip coupling using capped adiabatic tapered fibers. *APL Photonics* **5**(5), 056101 (2020).
- Barwicz, T. et al. Integrated metamaterial interfaces for self-aligned fiber-to-chip coupling in volume manufacturing. *IEEE J. Sel. Top. Quantum Electron.* **25**(3), 4700313 (2019).

12. Kohli, M. et al. C- and O-band dual-polarization fiber-to-chip grating couplers for silicon nitride photonics. *ACS Photonics* **10**(9), 3366–3373 (2023).
13. Blumenthal, D. J., Heideman, R., Geuzebroek, D., Leinse, A. & Roeloffzen, C. Silicon nitride in silicon photonics. *Proc. IEEE* **106**(12), 2209–2231 (2018).
14. Sharma, T. et al. Review of recent progress on silicon nitride-based photonic integrated circuits. *IEEE Access* **8**, 195436–195446 (2020).
15. Subramanian, A. Z. et al. Silicon and silicon nitride photonic circuits for spectroscopic sensing on-a-chip [Invited]. *Photonics Res.* **3**(5), B47–B59 (2015).
16. Muñoz, P. et al. Silicon nitride photonic integration platforms for visible, near-infrared and mid-infrared applications. *Sensors* **17**(9), 2088 (2017).
17. Son, G., Han, S., Park, J., Kwon, K. & Yu, K. High-efficiency broadband light coupling between optical fibers and photonic integrated circuits. *Nanophotonics* **7**(12), 1845–1864 (2018).
18. Marchetti, R., Lacava, C., Carroll, L., Grankowski, K. & Minzioni, P. Coupling strategies for silicon photonics integrated chips [Invited]. *Photonics Res.* **7**(2), 201–239 (2019).
19. Sapra, N. V. et al. Inverse design and demonstration of broadband grating couplers. *IEEE J. Sel. Top. Quantum Electron.* **25**(3), 6100207 (2019).
20. Papes, M. et al. Fiber-chip edge coupler with large mode size for silicon photonic wire waveguides. *Opt. Express* **24**(5), 5026–5038 (2016).
21. Zhu, X. et al. Low-loss fiber-to-chip edge coupler for silicon nitride integrated circuits. *Opt. Express* **31**(6), 10525–10532 (2023).
22. Ren, G., Chen, S., Cheng, Y. & Zhai, Y. Study on inverse taper based mode transformer for low loss coupling between silicon wire waveguide and lensed fiber. *Opt. Commun.* **284**(19), 4782–4788 (2011).
23. Bhandari, B. et al. Compact and broadband edge coupler based on multi-stage silicon nitride tapers. *IEEE Photonics J.* **12**(6), 6602511 (2020).
24. Wang, L. et al. CMOS-compatible, broadband, and polarization-independent edge coupler for efficient chip coupling with standard single-mode fiber. *Appl. Optics* **61**(26), 7798–7806 (2022).
25. Jiang, Y., Zhang, Z. & Liu, P. Broadband polarization-independent edge couplers with high efficiency based on SiN-Si dual-stage structure. *IEEE Photonics J.* **16**(2), 2200307 (2024).
26. Wu, D. et al. A theoretical sub-0.1 dB loss single mode fiber-to-chip edge coupler for silicon nitride waveguides. *Photonics* **10**(3), 231 (2023).
27. He, A., Guo, X., Wang, T. & Su, Y. Ultracompact fiber-to-chip metamaterial edge coupler. *ACS Photonics* **8**(11), 3226–3233 (2021).
28. Cheben, P. et al. Broadband polarization independent nanophotonic coupler for silicon waveguides with ultra-high efficiency. *Opt. Express* **23**(17), 22553–22563 (2015).
29. Li, Y. et al. Polarization insensitive edge coupler assisted by subwavelength grating and suspended structure. *IEEE Photonics Technol. Lett.* **34**(14), 765–768 (2022).
30. Xiao, Y., Xu, Y., Dong, Y., Zhang, B. & Ni, Y. A 60 μm -long fiber-to-chip edge coupler assisted by subwavelength grating structure with ultralow loss and large bandwidth. *Photonics* **9**(6), 413 (2022).
31. Mu, X. et al. Effects of fabrication deviations and fiber misalignments on a fork-shape edge coupler based on subwavelength gratings. *Opt. Commun.* **482**, 126562 (2021).
32. He, A. et al. Low loss, large bandwidth fiber-chip edge couplers based on silicon-on-insulator platform. *J. Lightwave Technol.* **38**(17), 4780–4786 (2020).
33. Teng, M. et al. Trident shape SOI metamaterial fiber-to-chip edge coupler. In *Optical fiber communication conference*, pp. Tu2J-6 (2019).
34. Bian, Y. et al. High-power, low-loss, fabrication tolerant multi-tip SiN edge coupler in 300mm monolithic SiPh foundry technology. In *Optical fiber communication conference*, pp.M4J-6 (2025).
35. Halir, R. et al. Recent advances in silicon waveguide devices using sub-wavelength gratings. *IEEE J. Sel. Top. Quantum Electron.* **20**(4), 8201313 (2014).
36. Wang, J., Glesk, I. & Chen, L. R. Subwavelength grating devices in silicon photonics. *Sci. Bull.* **61**(11), 879–888 (2016).
37. Mia, M. B., Jaidye, N., Ahmed, I., Ahmed, S. Z. & Kim, S. Broadband integrated polarization splitter and rotator using subwavelength grating claddings. *Opt. Express* **31**(3), 4140–4151 (2023).
38. Cheben, P., Halir, R., Schmid, J. H., Atwater, H. A. & Smith, D. R. Subwavelength integrated photonics. *Nature* **560**(7720), 565–572 (2018).
39. Li, Y., Lan, T., Li, J. & Wang, Z. High-efficiency edge-coupling based on lithium niobate on an insulator wire waveguide. *Appl. Optics* **59**(22), 6694–6701 (2020).

Author contributions

Sunwoo, Y. -H. and Lee, W. -B. conceived the idea, performed the numerical simulations, and discussed the results. Sunwoo, Y. -H. also drew and revised the figures. Kwon, Y. -J. did the experiment and analyzed the results. Im, C. -S. and Gwon, J. -Y. validated and interpreted the results. Oh, M. -C. and Lee, S. -S. guided in result analysis, data interpretation and supervised the whole work. All the authors contributed to the manuscript preparation.

Funding

Agency For Defense Development (ADD) funded by the Defense Acquisition Program Administration (DAPA) in 2023 (No.912905601); (UI220080TD).

Declarations

Competing interests

The authors declare no competing interests.

Additional information

Correspondence and requests for materials should be addressed to S.-S.L.

Reprints and permissions information is available at www.nature.com/reprints.

Publisher's note Springer Nature remains neutral with regard to jurisdictional claims in published maps and institutional affiliations.

Open Access This article is licensed under a Creative Commons Attribution-NonCommercial-NoDerivatives 4.0 International License, which permits any non-commercial use, sharing, distribution and reproduction in any medium or format, as long as you give appropriate credit to the original author(s) and the source, provide a link to the Creative Commons licence, and indicate if you modified the licensed material. You do not have permission under this licence to share adapted material derived from this article or parts of it. The images or other third party material in this article are included in the article's Creative Commons licence, unless indicated otherwise in a credit line to the material. If material is not included in the article's Creative Commons licence and your intended use is not permitted by statutory regulation or exceeds the permitted use, you will need to obtain permission directly from the copyright holder. To view a copy of this licence, visit <http://creativecommons.org/licenses/by-nc-nd/4.0/>.

© The Author(s) 2025